Revue des Composites et des Matériaux Avancés-Journal of Composite and Advanced Materials
Vol. 36, No. 1, February, 2026, pp. 1-11
Journal homepage: http://iieta.org/journals/rcma

From Filament to Functional Part: A Comparative Analysis of Structure-Property Relationships in 3D-Printed Coir Fiber Reinforced Polylactic Acid Biocomposites

Bakri Bakri, Muhammad Syaiful Fadly*, Sri Chandrabakty, Moch Ihtiar, Muh Ihwan

Department of Mechanical Engineering, Faculty of Engineering, Universitas Tadulako, Palu 94118, Indonesia

Corresponding Author Email: msfadly@untad.ac.id

https://doi.org/10.18280/rcma.360101

Received: 6 December 2025
Revised: 31 January 2026
Accepted: 15 February 2026
Available online: 28 February 2026

Keywords:
polylactic acid, coir fiber, biocomposites, fused deposition modeling, 3D printing, structure-property relationship, mechanical properties, thermal properties

ABSTRACT

The integration of natural fibers into polylactic acid (PLA) for fused deposition modeling (FDM) holds promise for sustainable additive manufacturing. However, a systematic understanding of how material properties evolve from the composite filament feedstock to the final printed part is lacking. This study bridges this gap by fabricating and comprehensively characterizing PLA biocomposite filaments reinforced with 0, 5, 7, and 9 wt.% sodium bicarbonate-treated coir fibers, followed by a critical comparison with their FDM-printed counterparts. Fourier-Transform Infrared Spectroscopy (FTIR) confirmed the preservation of chemical structures post-processing. X-ray diffraction analysis indicated that coir fibers acted as nucleating agents, enhancing PLA crystallinity with increasing fiber content. Thermogravimetric analysis revealed a marginal decrease in thermal stability attributed to the lignocellulosic nature of the fibers. Tensile testing showed that neat PLA filament exhibited the highest tensile strength (43.26 MPa), whereas the incorporation of coir fibers resulted in lower tensile strengths of 33.96 MPa (5 wt.%), 35.37 MPa (7 wt.%), and 35.22 MPa (9 wt.%). Notably, filaments consistently outperformed their 3D-printed versions across all compositions, primarily due to printing-induced anisotropy and interlayer voids. Scanning electron microscopy corroborated these findings, showing fiber agglomeration at higher contents (9 wt.%) and interfacial gaps that compromised stress transfer. The central conclusion is that for FDM-processed PLA/coir composites, process-induced defects exert a more dominant influence on mechanical performance than fiber reinforcement itself, especially at higher fiber contents. This underscores the necessity for concurrent optimization of material formulation and printing parameters to harness the full potential of these sustainable biocomposites in additive manufacturing.

1. INTRODUCTION

In the past decade, additive manufacturing (AM), also referred to as three-dimensional (3D) printing, has undergone remarkable development and has become a key area of interest in both academic research and industrial practice. This manufacturing paradigm enables the direct fabrication of components with complex geometries, high design flexibility, and shortened development cycles using a wide variety of polymer-based feedstocks [1-3]. Among the available AM technologies, fused deposition modelling (FDM) has achieved the most significant level of industrial adoption owing to its straightforward processing principle, relatively low equipment and operating costs, efficient material use, and the widespread commercial availability of thermoplastic filaments [4]. In FDM, a solid thermoplastic filament is continuously fed into a heated extrusion nozzle, where it is melted and deposited sequentially in a layer-by-layer fashion to form three-dimensional objects [5]. Polymers commonly processed via FDM include polylactic acid (PLA), polystyrene (PS), acrylonitrile butadiene styrene (ABS), and polycarbonate (PC), representing both biodegradable and conventional thermoplastic materials suitable for additive manufacturing applications [6-9].

PLA is among the most intensively studied thermoplastic polymers for FDM owing to its favorable melt processability, balanced mechanical performance, biocompatibility, intrinsic biodegradability, and high optical clarity [6, 10]. Nevertheless, the broader application of PLA in load bearing or thermally demanding environments is restricted by several inherent shortcomings, including limited thermal stability, slow crystallization behavior, low fracture strain, and inadequate flexibility [11, 12]. In response to these limitations, current research efforts have increasingly shifted toward the formulation of PLA-based composite systems by incorporating reinforcing phases. A growing body of literature has demonstrated that integrating natural fibers, nanocellulose, hydroxyapatite, pulp fibers, and various organic or inorganic particulate reinforcements can substantially enhance the mechanical, thermal, and functional properties of PLA, thereby extending its applicability in advanced engineering [13-16].

Natural fibers have gained increasing interest as reinforcements for biopolymer composites due to their renewability, biodegradability, non-toxicity, and low environmental impact. Materials such as jute, sisal, hemp, banana, pineapple leaf fibers, and coir are widely used to reduce carbon footprint while improving composite sustainability. To strengthen fiber matrix interfacial adhesion, various surface modification techniques, including alkali, peroxide, and permanganate treatment, are commonly applied to improve compatibility at the interface [17-19]. Among these natural fiber candidates, coir stands out as a promising reinforcement for PLA-based composites owing to its low density, low thermal conductivity, and cost-effectiveness, making it suitable for lightweight structural applications [20]. Coir also exhibits strong acoustic absorption and favorable resistance to moisture and biological degradation, both of which are attributed to its lignocellulosic composition. Chemically, coir contains moderate cellulose (36-43%), low hemicellulose content, and a relatively high lignin fraction (41-45%), which contributes to its large microfibril angle and results in fibers with lower tensile strength but remarkably high elongation at break [21-23]. These characteristics make coir particularly attractive for applications where toughness and damage tolerance are critical rather than high stiffness alone. Traditionally used in ropes, mats, and household products [24], coir fiber has more recently been incorporated into acoustic panels, thermal insulation materials, construction components, and automotive parts. This expanding range of applications underscores its potential as an environmentally sustainable reinforcement for the development of lightweight and durable PLA biocomposites [25-27].

Extensive research has examined coir-reinforced green composites, demonstrating their effectiveness in enhancing the performance of various biodegradable polymer systems. For PLA-based composites, Dong et al. [28] investigated materials containing 5-30 wt.% coir fibers fabricated via hydraulic pressing. Their findings indicated that increasing fiber content generally reduced tensile and flexural properties. NaOH-treated fibers significantly improved overall mechanical performance, with the highest strength observed at 20 wt.% fiber content. Similarly, Nam et al. [22] developed biodegradable PBS/coir composites and reported that immersing coir fibers in 5% NaOH solution for 72 h increased the interfacial shear strength by 55.6%, resulting in stiffer and stronger composites. Brahmakumar et al. [29] further demonstrated that inadequate fiber surface modification severely degrades fiber–matrix adhesion, leading to pronounced reductions in tensile modulus and strength. While these studies clearly establish the importance of fiber treatment and fiber content, they are mainly limited to bulk-processed or compression-molded composites and do not account for the additional complexities introduced by filament extrusion and layer-by-layer deposition in FDM.

Critically, despite the increasing use of natural fiber–reinforced PLA in additive manufacturing, systematic investigations addressing the fabrication of reinforced filaments and the subsequent evolution of properties during the FDM printing process remain scarce. Most existing studies evaluate only the final printed components or bulk specimens, thereby overlooking the distinct roles of filament quality, extrusion-induced fiber alignment, and printing-induced anisotropy and interlayer void formation. As a result, the transition in material properties from the filament stage to the final printed part remains insufficiently understood for PLA/coir systems. To address this gap, the present study provides a direct, systematic comparison of extruded PLA/coir biocomposite filaments and their corresponding FDM-printed specimens. Filaments containing 0, 5, 7, and 9 wt.% coir fiber were produced via single-screw extrusion to examine the influence of fiber incorporation on the mechanical, thermal, and structural properties of the composites. Fourier-Transform Infrared (FTIR), X-ray diffraction (XRD), and TGA analyses were conducted to evaluate chemical structure, crystallinity, and thermal behavior. In addition, scanning electron microscopy (SEM) observations were performed on both extruded filaments and 3D-printed specimens to assess fiber dispersion and fiber–matrix interfacial integrity. By explicitly linking filament characteristics to printing-induced microstructural features and mechanical performance, this work aims to clarify the dominant factors governing the performance limitations of PLA/coir biocomposites in FDM applications.

2. MATERIALS AND METHODS

2.1 Materials

SUNLU PLA + 2.0 served as the polymer matrix in this study. The material was supplied as pellets with a nominal filament diameter of 1.75 mm and a density of 1.24 g/cm³ and was imported from the United States. Coir fibers obtained from Donggala Regency, Central Sulawesi, Indonesia, functioned as the reinforcing phase. The fibers exhibited a density of 1.15 g/cm³ and an average diameter of 100-200 μm. Sodium bicarbonate ($NaHCO_3$), pro analysis grade, supplied by Merck (Germany), was employed as the chemical reagent.

2.2 Fiber treatment

Coir fibers were mechanically extracted from coconut husks and subsequently washed under running water to remove residual impurities. The fibers were then treated with a sodium bicarbonate ($NaHCO_3$) solution, a method reported in previous studies to preserve fiber integrity and enhance tensile performance [30]. To leverage this optimal condition, the fibers in the present study were immersed in a 12 wt.% $NaHCO_3$ solution for 24 h at ambient temperature. After the treatment, the fibers were rinsed with distilled water until the pH was neutral, then dried in an oven at 115°C for 1 h. The dried fibers were subsequently cut to 5-7 mm, ground to a fine powder, and sieved through a 200-mesh screen to obtain a uniform particle size suitable for subsequent compounding. Figure 1 presents an overview of the fiber treatment process.

2.3 Filament fabrication and three-dimensional printed samples

Before extrusion, coconut shell fibers after being sieved through a 200-mesh screen were oven-dried at 65°C for 3 h to minimize moisture content and prevent hydrolytic degradation during processing. The dried fibers were subsequently blended with PLA pellets in a milling mixer to prepare composite feedstocks containing 5, 7, and 9 wt.% coir fiber. Neat PLA (0 wt.% fiber) and the prepared composite feedstocks were then processed using a Wellzoom single-screw desktop extruder (China). The extrusion process employed a barrel temperature of 147°C, an extrusion speed of 1200 mm/min, and a target

filament diameter of 1.75 mm. The extrusion process yielded four types of filaments, neat PLA (0 wt.% coir), which served as the reference material, and PLA/5% coir, PLA/7% coir, and PLA/9% coir. All extruded filaments were cooled under ambient conditions, collected, and stored for subsequent mechanical and physical characterization.

Tensile test specimens were fabricated in accordance with ASTM D638-22 [31, 32]. The specimen geometry was designed using computer-aided design (CAD) software and prepared for printing using OrcaSlicer. For each formulation, seven specimens were manufactured using a Kingroon KP3S FDM 3D printer (China). The printing process employed a nozzle diameter of 0.3 mm, a nozzle temperature of 250°C, a bed temperature of 70°C, a layer height of 0.2 mm, and an infill density of 100%. Figure 2 presents a schematic representation of the filament preparation and specimen fabrication workflow.

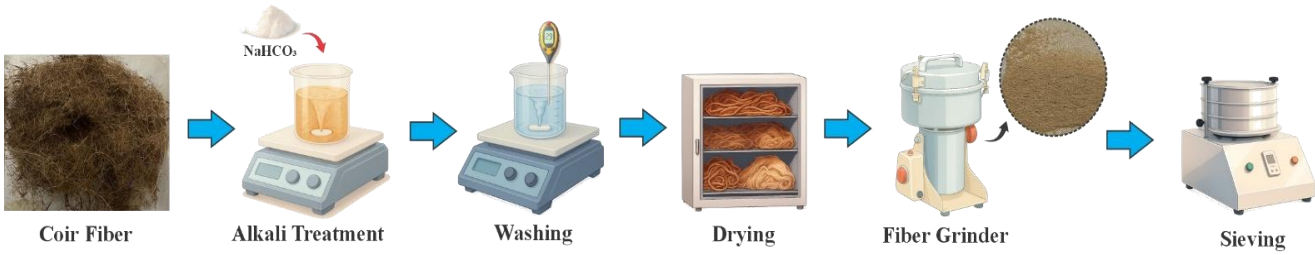

Figure 1. Treatment process of coir fibers

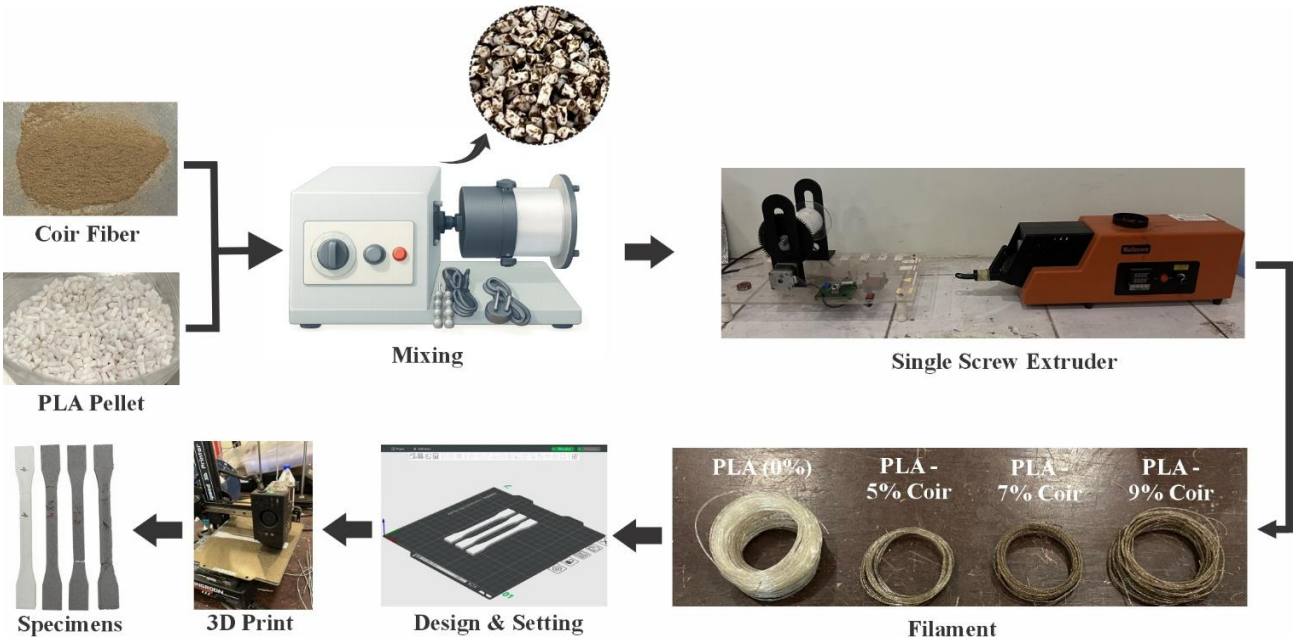

Figure 2. Process schematic for filament manufacturing and three-dimensional (3D) printing of test samples

3. CHARACTERIZATION

3.1 Scanning electron microscopy and X-ray spectroscopy

A JSM-IT700HR SEM (JEOL Ltd.), operated at an accelerating voltage of 10 kV, was used to examine the surfaces of the extruded filaments. The instrument was equipped with an energy-dispersive X-ray spectroscopy (EDS) system to perform quantitative elemental analysis. In addition, the fracture surfaces of tensile-tested 3D-printed specimens were analyzed by SEM to characterize the failure mechanisms and to evaluate fiber–matrix interfacial behavior.

3.2 Fourier-transform infrared

A Shimadzu IRAffinity-1S FT-IR spectrometer (Japan) was used to characterize the chemical structures of the coir-reinforced PLA biocomposite filaments over a wavenumber range of 500-4000 cm^{-1}.

3.3 X-ray diffraction

A Rigaku MiniFlex 600 X-ray diffractometer was used to analyze the crystalline structures of neat PLA, coir fibers, and the corresponding composite filaments. The measurements were performed over a 2θ range of 0-50° to characterize the phase composition and crystallinity of the samples.

3.4 Thermogravimetric analysis

A Hitachi STA7300 thermogravimetric analyzer (Japan) was used to evaluate the thermal behavior and stability of the samples. Specimens containing different coir fiber contents were heated from 25°C to 600°C at a heating rate of 10°C/min under a nitrogen flow rate of 50 mL/min to investigate the effect of fiber incorporation on the thermal degradation characteristics.

3.5 Tensile properties

A universal testing machine (Universal Testing Machine (UTM)), TN-MD equipped with a 200 kN load cell was used to determine the tensile properties of the specimens. The tests were conducted at a crosshead speed of 1 mm/min, and seven specimens were evaluated for each formulation to ensure the statistical reliability and reproducibility of the results, as shown in Figure 3.

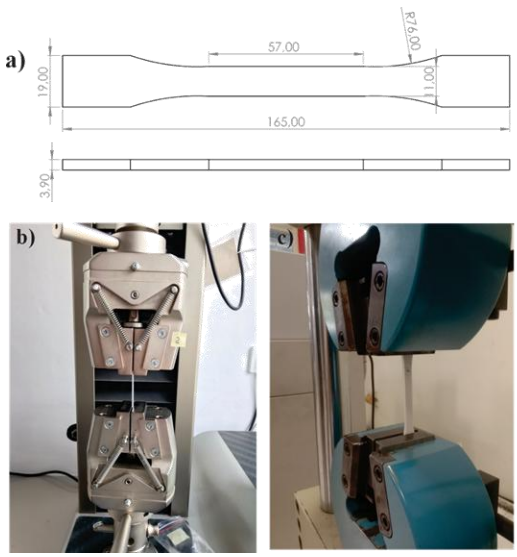

Figure 3. Sample design and mechanical testing setup: a) specimen design for tensile test, b) tensile test of filament, c) tensile test of three-dimensional (3D)-printed

4. RESULTS AND DISCUSSION

4.1 Scanning electron microscopy and X-ray spectroscopy analysis

Figure 4(a) illustrates the smooth and homogeneous surface morphology of neat PLA. At the same time, EDS analysis reveals carbon and oxygen contents of 44.9 wt.% and 55.1 wt.%, respectively, which are consistent with the expected chemical composition of PLA. The incorporation of 5 wt.% coir fibers (Figure 4(b)) increases surface roughness and introduces light–dark contrasts indicative of cellulose-rich regions at a coir fiber content of 7 wt.% (Figure 4(c)), the fibers exhibit a more uniform dispersion within the PLA matrix. In contrast, at a coir fiber content of 9 wt.% (Figure 4(d)), pronounced fiber agglomeration is observed, which is associated with an increased O/C ratio of 1.22, indicative of the higher cellulose content.

The limited fiber dispersion observed at higher fiber contents supports the findings of dos Santos et al. [33], who reported that elevated natural fiber fractions reduce composite homogeneity and promote the formation of interfacial voids or weak interfacial regions. These microstructural defects act as stress concentrators, reducing the composite's effective load-bearing cross-sectional area and contributing to the decrease in elastic modulus and tensile strength observed at higher fiber contents (Figure 4-11). In addition, SEM observations of the fracture surfaces reveal voids in all filaments formed during the extrusion process. These voids originate from the expansion of the molten material as it exits the extrusion nozzle under pressure gradients, consistent with previous reports [34-36].

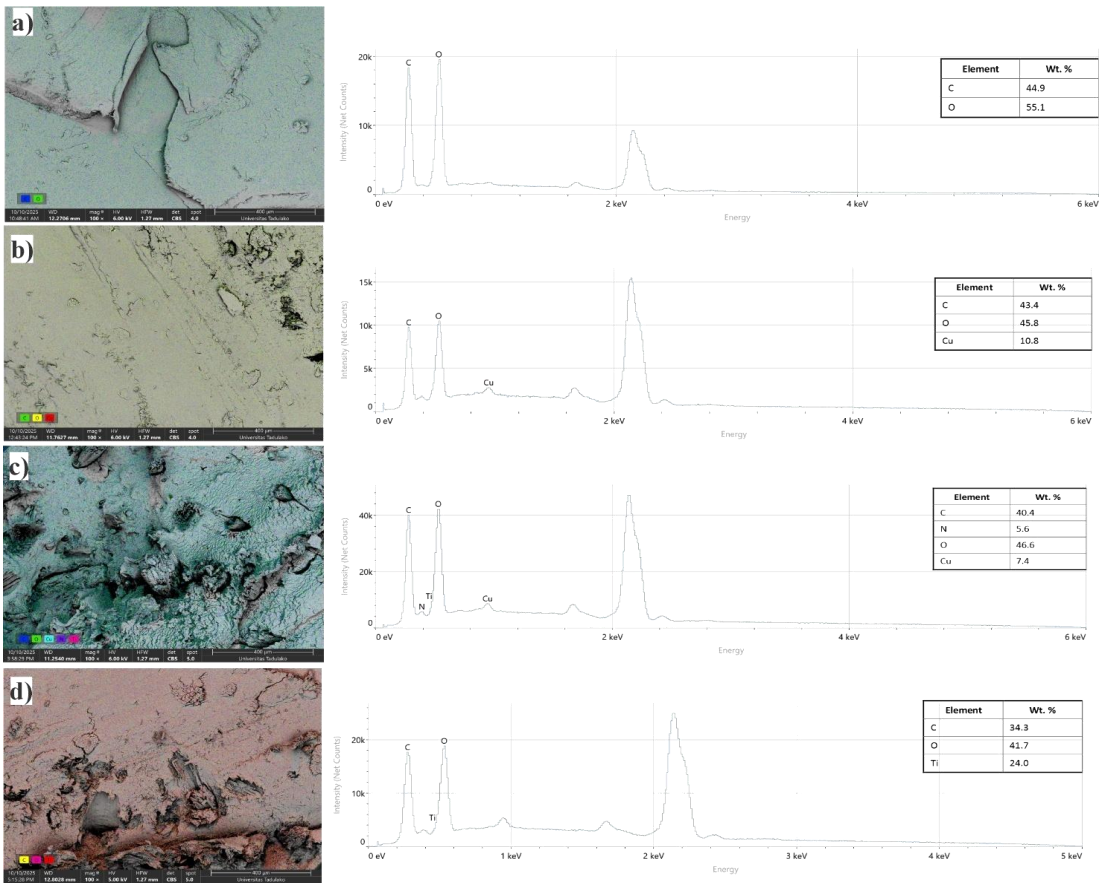

Figure 4. Surface morphology and X-ray spectroscopy (EDS) compositional mapping of a) neat polylactic acid (PLA), b) PLA/5% coir, c) PLA/7% coir, and d) PLA/9% coir

4.2 Diameter measurements of filament

Table 1 summarizes the measured filament diameters. Neat PLA filaments exhibited a diameter of 1.75 mm. In contrast, the coir-reinforced filaments ranged from 1.72 to 1.83 mm, indicating that the incorporation of coir fibers induced only minor changes in filament dimensions. This behavior can be attributed to the physical properties of the coir powder, which affect melt flow and filler–matrix interactions [37], consistent with previous observations in PLA/PCL filaments reinforced with hydroxyapatite [38]. All filament diameters remained close to the nominal 1.75 mm nozzle size, with slight deviations arising from natural shrinkage during cooling [39] or from extrusion parameters such as applied force, melt viscosity, temperature, and screw speed [40, 41]. Overall, the observed diameter variations (0-4.57%) fall within acceptable tolerances for FDM printing.

Table 1. Filament diameters of biocomposites with varying fiber contents

Sample	Coir Content (wt.%)	Diameter (mm)
Neat polylactic acid (PLA)	0	1.75 ± 0.007
PLA/5% Coir	5	1.72 ± 0.009
PLA/7% Coir	7	1.82 ± 0.041
PLA/9% Coir	9	1.83 ± 0.014

4.3 Fourier-transform infrared analysis

Figure 5 presents the FTIR spectra of neat PLA, coir fibers, and PLA/coir composite filaments containing 0, 5, 7, and 9 wt.% fiber. The coir fibers exhibit characteristic lignocellulosic absorption bands, including a broad hydroxyl (–OH) stretching vibration at 3333 cm^{-1} and C–H stretching vibrations at approximately 2937 cm^{-1}. Additional absorption peaks at 1452, 1382, and 1240 cm^{-1} correspond to CH_2 bending, C–H deformation, and asymmetric C–O–C stretching vibrations, respectively, which are associated with cellulose and hemicellulose components [39-42]. In contrast, the FTIR spectrum of neat PLA shows distinct absorption bands at 1745, 1452, 1180, 1080, and 869 cm^{-1}, which are assigned to C=O stretching, C–O stretching, CH bending, and C–C skeletal vibrations, thereby confirming the molecular structure of the polymer [41, 42]. The FTIR spectra of the PLA/coir composite filaments closely resemble that of neat PLA, indicating that the incorporation of coir fibers does not induce chemical modification of the PLA matrix.

However, peak intensity increases with increasing fiber content. The –OH band at 3333 cm^{-1} broadens and intensifies, reflecting the hydrophilic hydroxyl groups originating from cellulose and hemicellulose [40, 41]. CH-related vibrations at 2998 and 2945 cm^{-1} and the C=O stretching at 1745 cm^{-1} remain clearly discernible [40-42]. A minor peak near 1622 cm^{-1}, attributed to moisture absorption [41, 42], becomes more prominent in the composites, consistent with the hygroscopic nature of lignocellulosic fibers. Peaks at 1452 and 1382 cm^{-1}, corresponding to CH_3 bending, increase with fiber content, confirming the contribution of the cellulose-rich filler [40].

4.4 X-ray diffraction analysis

Figure 6 presents the XRD patterns of biocomposite filaments containing 0, 5, 7, and 9 wt.% coir fiber. The coir fibers exhibit characteristic cellulose I diffraction peaks at $2\theta \approx$ 15-6°, 22-23°, and 34°, corresponding to the 110, 200, and 004 crystallographic planes and confirming their semicrystalline structure [42-44]. Neat PLA shows distinct diffraction peaks at 16.5° and 19.5°, indicating its inherent semicrystalline nature [45, 46]. The PLA/coir composite filaments retain the primary crystalline features of PLA. In contrast, the increasing intensity of the 16.5° peak with higher coir fiber content suggests that the coir fibers act as nucleating agents and promote enhanced crystallinity within the PLA matrix [34].

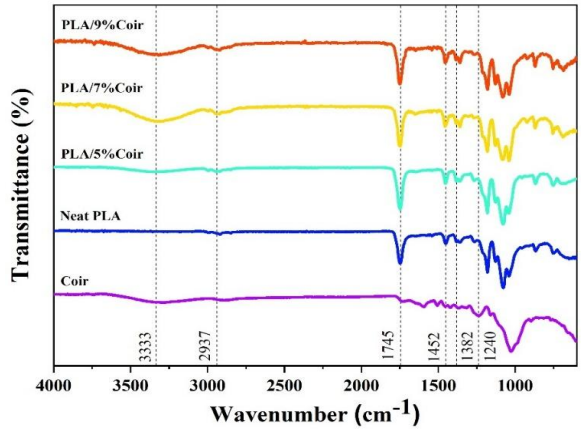

Figure 5. Fourier-Transform Infrared Spectroscopy (FTIR) spectra of coir, neat polylactic acid (PLA) and PLA/Coir fiber filaments with different coir contents

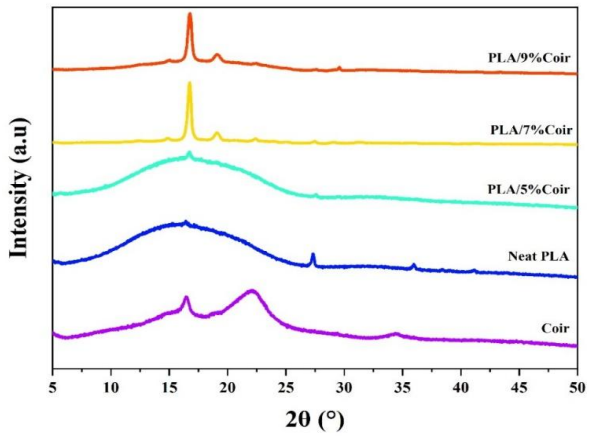

Figure 6. X-ray diffraction (XRD) patterns of coir, neat polylactic acid (PLA) and PLA/Coir fiber filaments with different coir contents

The enhancement in crystallinity arises from the restricted mobility of PLA chains caused by interfacial interactions with cellulose in the coir fibers. Hydrogen bonding between the hydroxyl (–OH) groups of the coir fibers and the polar functional group of PLA forms a stiffer interfacial region, which promotes the nucleation of numerous small crystalline domains that are commonly associated with transcrystalline structures in natural fiber–reinforced composites [47]. This mechanism is consistent with the findings of Tao et al. [48], who reported that lignocellulosic fillers increase PLA crystallinity. At higher fiber contents (7-9 wt.%), the diffraction peak intensities further increase, indicating the formation of additional nucleation sites on the fiber surfaces. The large surface area of the coir fibers facilitates extensive nucleation, leading to the development of overlapping small

crystalline domains, restricting spherulite growth, and resulting in a denser, more fragmented, and thermally stable crystalline structure [49].

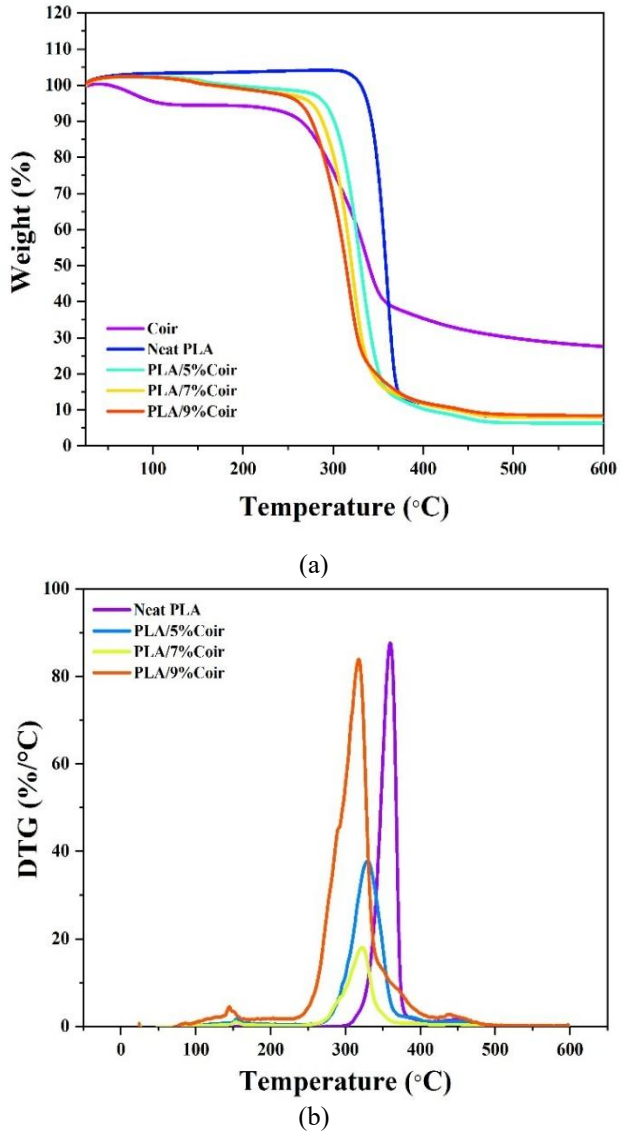

Figure 7. a) Thermogravimetric analysis (TGA) and b) derivative thermogravimetric (DTG) curves of PLA/coir biocomposite filaments at varying coir contents

4.5 Thermal analysis results (TGA)

Figure 7(a) illustrates the thermogravimetric behavior of coir fibers, which undergo three principal degradation stages typical of lignocellulosic materials: moisture loss (25-150°C), hemicellulose decomposition (190-290°C), and cellulose depolymerization (290-360°C), while lignin decomposes over a broader temperature range (280-500°C) due to its aromatic structure [50, 51]. Neat PLA exhibits a single, sharp degradation peak with a maximum degradation temperature (T_{max}) of 360.67°C (Figure 7(b)), indicative of rapid chain scission within its semi-crystalline structure.

In PLA/coir biocomposites, T_{max} progressively decreases with increasing coir content (5-9 wt.%), reflecting reduced thermal stability attributable to the lower thermal resistance of lignocellulosic fibers. Similar trends have been observed in PLA composites reinforced with sisal and phormium fibers, where early degradation of the natural fibers accelerates overall mass loss [52, 53]. For composites with low fiber contents, TGA patterns remain dominated by PLA, consistent with reports on other low-fiber-content natural fiber composites [54, 55]. The derivative thermogravimetric (DTG) curves (Figure 7(b)) further confirm that T_{max} decreases with increasing coir content. Lignocellulosic fibers degrade at lower temperatures than PLA, leading to earlier mass loss, and the hydroxyl-rich groups in cellulose and hemicellulose contribute to this reduction in degradation temperature. Additionally, interfacial interactions between PLA and coir may restrict polymer chain mobility, influencing the thermal behavior of the composites. At higher fiber contents (7-9 wt.%), DTG peaks broaden, reflecting the overlapping degradation of PLA and coir components. Despite the reduction in thermal stability, the composites exhibit slightly higher residual mass at 600°C, consistent with other natural fiber systems [56].

Table 2. Thermal behaviour of coir fiber, neat polylactic acid (PLA), and PLA/coir biocomposites

Sample	T_{onset} (°C)	T_{max} (°C)	$W_{residue}$ (%)
Coir	294.30	338.16	8.77
Neat PLA	342.10	360.67	10.83
PLA/5% Coir	302.60	330.59	6.21
PLA/7% Coir	293.80	321.93	4.46
PLA/9% Coir	280.80	316.45	8.16

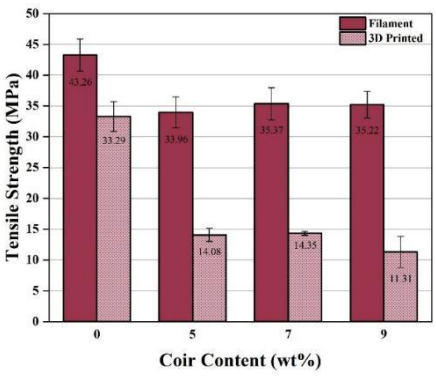

Figure 8. Tensile strength of filaments and three-dimensional (3D)-printed

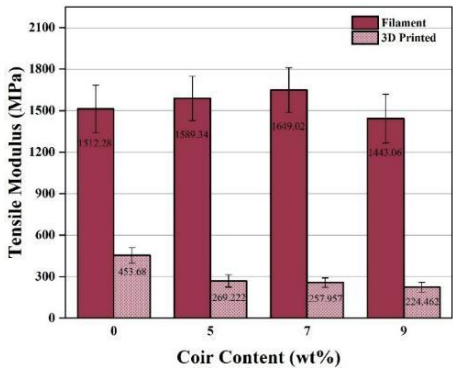

Figure 9. Tensile modulus of filaments and three-dimensional (3D)-printed

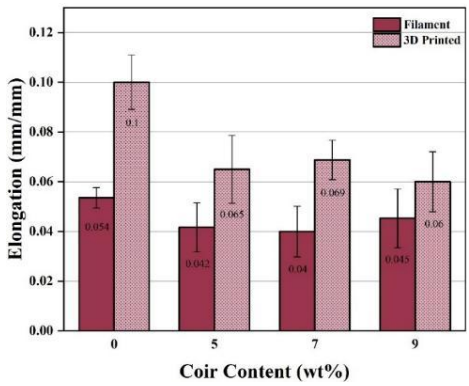

Figure 10. Elongation at break of filaments and three-dimensional (3D)-printed

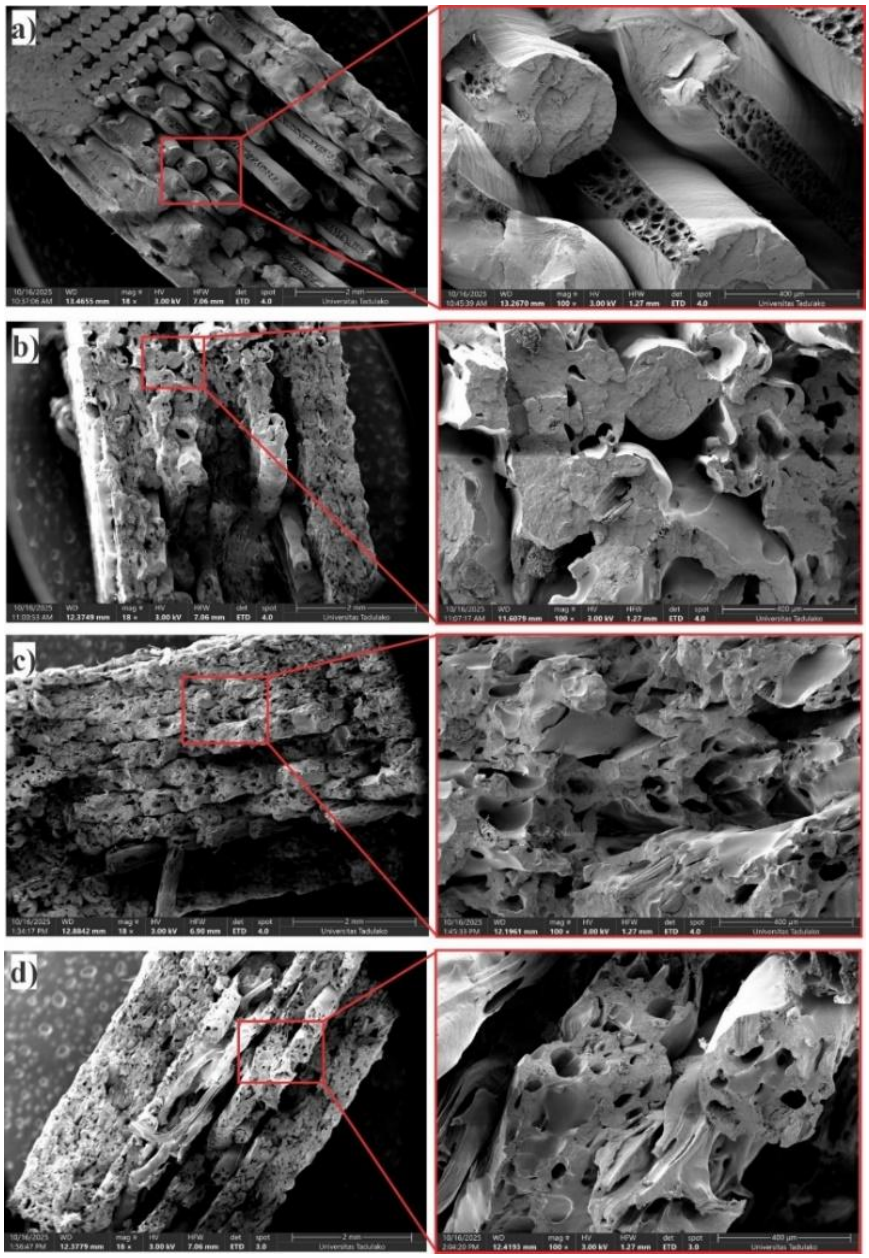

Figure 11. Scanning electron microscopy (SEM) micrographs of the fracture surfaces of (a) neat PLA, (b) PLA/5 wt.% coir, (c) PLA/7 wt.% coir, and (d) PLA/9 wt.% coir biocomposites at magnifications of 18× and 100×

The onset temperatures (T_{onset}) presented in Table 2 justify these observations. Coir fibers exhibit T_{onset} of 294.30°C, neat PLA 342.10°C, and PLA/coir composites show a progressive decrease with increasing fiber content: PLA/5 % at 302.60°C, PLA/7 % at 293.80°C, and PLA/9 % at 280.80°C. These trends are consistent with those observed in PLA/cellulose nanocrystal composites, where low-molecular-weight components such as hemicellulose and lignin induce early weight loss [14]. T_{max} follows a similar pattern, decreasing from 360.67°C for neat PLA to 330.59, 321.93, and 316.45°C for 5, 7, and 9 wt.% coir, respectively. Residual mass ($W_{residue}$) in the composites ranges from 4.46-8.16 %, reflecting the interplay between PLA and coir during pyrolysis.

4.6 Tensile properties of filaments and three-dimensional-printed specimens

Figure 8 illustrates that the tensile strength of the filaments decreases with increasing coir fiber content. For each composition and processing condition, tensile properties were determined from at least seven specimens, and the reported values correspond to the standard deviation. Neat PLA exhibits the highest tensile strength (43.26 MPa), whereas composites containing 5-9 wt.% coir demonstrate reduced strengths, reaching 35.37 MPa at 7 wt.% and 35.22 MPa at 9 wt.%. The reduction in mechanical performance results from the lower intrinsic strength of lignocellulosic fibers and the presence of interfacial defects, such as voids and fiber pull-out, consistent with previous studies on natural fiber–reinforced PLA composites and evidenced by the SEM observations shown in Figure 11. The 3D-printed specimens exhibit further decreases in tensile strength due to anisotropy and interlayer voids that act as stress concentrators, thereby limiting molecular entanglement between adjacent printed layers [57-59].

Figure 9 illustrates that the tensile modulus of the filaments initially increases with the incorporation of coir fibers, reaching a maximum of 1649.02 MPa at 7 wt.% coir, before decreasing to 1443.06 MPa at 9 wt.%. At moderate fiber contents, the PLA matrix is effectively stiffened due to

efficient stress transfer between the matrix and the fibers [28]. In contrast, higher fiber contents promote fiber agglomeration, inadequate wetting, and the formation of voids, which collectively reduce stiffness, consistent with observations in high-fiber-content natural fiber composites [28, 58]. Across all compositions, the 3D-printed specimens exhibit lower tensile modulus than their filament counterparts, attributed to interlayer gaps and internal porosity [60, 61].

Figure 10 demonstrates that neat PLA exhibits the highest ductility, whereas the rigid coir fibers restrict polymer chain mobility. A slight increase in elongation at break for 3D-printed composites containing 7-9 wt.% coir may be attributed to fiber bundles facilitating localized deformation [58]. Nevertheless, the printed specimens remain less ductile than the filaments, reflecting the influence of interlayer defects and voids that promote premature crack initiation, as similarly reported for PLA/cellulose nanocrystal and PLA/recycled-paper composites [62, 63].

4.7 Morphological structures

Figure 11(a) shows that neat PLA exhibits layer lines, interlayer cracks, and small voids resulting from incomplete interlayer fusion, which leads to brittle fractures along the printing direction. These microstructural features are consistent with previous reports indicating that deficiencies in interlayer bonding in FDM-printed PLA act as primary sites for crack initiation and consequently reduce tensile strength [64].

Figures 11(b-d) illustrate the fracture surfaces of the PLA/coir composite specimens. Fiber pull-out generates voids in all composite samples, while the composite containing 5 wt.% coir (Figure 11(b)) exhibits partial PLA–coir interfacial bonding. At a coir fiber content of 7 wt.% (Figure 11(c)), numerous cavities indicate limited matrix wetting and weak fiber–matrix adhesion. In addition, partial fiber breakage and fiber pull-out are observed, reflecting modest improvements in stress transfer and consistent with the findings reported by Dong et al. [28]. At a coir fiber content of 9 wt.% (Figure 11(d)), larger fiber clusters and agglomerates act as stress concentrators, reducing tensile strength and tensile modulus, as shown in Figures 8 and 9. These microstructural features facilitate crack propagation, disrupt interlayer fusion, and produce irregular fracture patterns, which are consistent with prior studies [65].

5. CONCLUSIONS

The key finding of this study is that process-induced constraints more strongly influence the mechanical performance of FDM-printed PLA/coir biocomposites than fiber addition. SEM observations revealed interfacial voids, fiber pull-out, and incomplete interlayer fusion, which act as stress concentrators and limit effective load transfer. Consequently, despite enhanced crystallinity at low fiber contents, all PLA/coir composites exhibited lower tensile strength than neat PLA. At coir fiber contents of 5-7 wt.%, improved fiber dispersion and nucleation-induced crystallinity resulted in moderate increases in tensile modulus, whereas a higher fiber content of 9 wt.% promoted agglomeration and porosity, leading to reductions in both tensile strength and stiffness. These results demonstrate that FDM-related defects at higher fiber contents progressively outweigh the beneficial effects of fiber reinforcement. The central implication of this work is that effective optimization of natural fiber–reinforced PLA for FDM applications requires the co-design of material formulations and printing parameters, as composite performance cannot rely solely on fiber incorporation but must also address extrusion stability, filament quality, and interlayer fusion to exploit sustainable biocomposites in additive manufacturing fully.

ACKNOWLEDGMENT

The authors would like to thank the Indonesian Ministry of Higher Education, Science, and Technology (Kemendiktisaintek RI) for the research funding support.

REFERENCES

[1] Srivastava, M., Rathee, S. (2022). Additive manufacturing: Recent trends, applications and future outlooks. Progress in Additive Manufacturing, 7(2): 261-287. https://doi.org/10.1007/s40964-021-00229-8

[2] Chattopadhyay, S., Mahapatra, S.D., Mandal, N.K. (2024). Advancements and challenges in additive manufacturing: A comprehensive review. Engineering Research Express, 6(1): 12505. https://doi.org/10.1088/2631-8695/ad30b1

[3] Hajare, D.M., Gajbhiye, T.S. (2022). Additive manufacturing (3D printing): Recent progress on advancement of materials and challenges. Materials Today: Proceedings, 58(2): 736-743. https://doi.org/10.1016/j.matpr.2022.02.391

[4] Solomon, I.J., Sevvel, P., Gunasekaran, J. (2021). A review on the various processing parameters in FDM. Materials Today: Proceedings, 37(2): 509-514. https://doi.org/10.1016/j.matpr.2020.05.484

[5] Acierno, D., Patti, A. (2023). Fused deposition modelling (FDM) of thermoplastic-based filaments: Process and rheological properties—An overview. Materials, 16(24): 7664. https://doi.org/10.3390/ma16247664

[6] Sandanamsamy, L., Harun, W.S.W., Ishak, I., Romlay, F.R.M., Kadirgama, K., Ramasamy, D., Idris, S.R.A., Tsumori, F. (2023). A comprehensive review on fused deposition modelling of polylactic acid. Progress in Additive Manufacturing, 8(5): 775-799. https://doi.org/10.1007/s40964-022-00356-w

[7] Taresh, O.F., Mezher, M.T., Daway, E.G. (2023). Mechanical properties of 3D-printed PETG samples: The effect of varying infill patterns. Revue des Composites et des Matériaux Avancés-Journal of Composite and Advanced Materials, 33(5): 339-345. https://doi.org/10.18280/rcma.330508

[8] Gorana, F., Modi, Y.K. (2024). Process parameter optimization for fabrication of acrylonitrile butadiene styrene parts. Materials Today: Proceedings, 103: 109-114. https://doi.org/10.1016/j.matpr.2023.08.204

[9] Cicek, U.I., Johnson, A.A. (2025). Multi-objective optimization of FDM process parameters for 3D-printed polycarbonate using Taguchi-based Gray Relational Analysis. The International Journal of Advanced Manufacturing Technology, 137: 3709-3725. https://doi.org/10.1007/s00170-025-15392-3

[10] Plamadiala, I., Croitoru, C., Pop, M.A., Roata, I.C.

(2025). Enhancing polylactic acid (PLA) performance: A review of additives in fused deposition modelling (FDM) filaments. Polymers, 17(2): 191. https://doi.org/10.3390/polym17020191

[11] Andrzejewski, J., Das, S., Lipik, V., Mohanty, A.K., Misra, M., You, X., Tan, L.P., Chang, B.P. (2024). The development of poly (lactic acid) (PLA)-based blends and modification strategies: Methods of improving key properties towards technical applications. Materials, 17(18): 4556. https://doi.org/10.3390/ma17184556

[12] Tripathi, N., Misra, M., Mohanty, A.K. (2021). Durable polylactic acid (PLA)-based sustainable engineered blends and biocomposites: Recent developments, challenges, and opportunities. ACS Engineering Au, 1(1): 7-38. https://doi.org/10.1021/acsengineeringau.1c00011

[13] Kacem, M.A., Guebailia, M., Dezaki, M.L., Abdi, S., Sabba, N., Zolfagharian, A., Bodaghi, M. (2025). Development and 3D printing of PLA bio-composites reinforced with short yucca fibers and enhanced thermal and dynamic mechanical performance. Journal of Materials Research and Technology, 36: 1243-1258. https://doi.org/10.1016/j.jmrt.2025.03.184

[14] Ahmad, N.D., Wildan, M.W. (2023). Preparation and properties of cellulose nanocrystals-reinforced Poly (lactic acid) composite filaments for 3D printing applications. Results in Engineering, 17: 100842. https://doi.org/10.1016/j.rineng.2022.100842

[15] Mathiazhagan, N., Palaniyappan, S., kumar Sivakumar, N. (2023). Effect of fused filament fabrication parameters on crashworthiness studies of hydroxyapatite particle reinforced PLA composite thin-walled tubes. Journal of the Mechanical Behavior of Biomedical Materials, 138: 105611. https://doi.org/10.1016/j.jmbbm.2022.105611

[16] Du, J., Hu, Y., Hu, S. (2024). Interfacial control and dispersion characteristics of polylactic acid fiber/pulp fiber composites. Polymer Composites, 45(10): 8970-8983. https://doi.org/10.1002/pc.28388

[17] Arunachalam, S.J., Saravanan, R., Anbuchezhiyan, G. (2024). An overview on chemical treatment in natural fiber composites. Materials Today: Proceedings. https://doi.org/10.1016/j.matpr.2024.05.108

[18] 1Varma, M., Chandran, S. (2025). Surface treatment of natural fibers for enhancing interfacial adhesion and mechanical properties in biocomposites—A comprehensive review. Composite Interfaces, 1-37. https://doi.org/10.1080/09276440.2025.2498795

[19] AL-Oqla, F.M., Alaaeddin, M.H. (2022). Chemical modifications of natural fiber surface and their effects. In Bast Fibers and Their Composites: Processing, Properties and Applications, pp. 39-64. https://doi.org/10.1007/978-981-19-4866-4_3

[20] Chamola, R., Das, S., Ahlawat, D.S., Mishra, Y.K., Goyat, M.S. (2024). Recent developments in shear thickening fluid-impregnated synthetic and natural fiber-reinforced composites for ballistic applications: A review. Journal of Materials Science, 59(3): 747-793. https://doi.org/10.1007/s10853-023-09201-z

[21] Nam, T.H., Ogihara, S., Tung, N.H., Kobayashi, S. (2011). Effect of alkali treatment on interfacial and mechanical properties of coir fiber reinforced poly (butylene succinate) biodegradable composites. Composites Part B: Engineering, 42(6): 1648-1656. https://doi.org/10.1016/j.compositesb.2011.04.001

[22] Nam, T.H., Ogihara, S., Kobayashi, S. (2012). Interfacial, mechanical and thermal properties of coir fiber-reinforced poly (lactic acid) biodegradable composites. Advanced Composite Materials, 21(1): 103-122. https://doi.org/10.1163/156855112X629540

[23] Adeniyi, A.G., Onifade, D.V., Ighalo, J.O., Adeoye, A.S. (2019). A review of coir fiber reinforced polymer composites. Composites Part B: Engineering, 176: 107305. https://doi.org/10.1016/j.compositesb.2019.107305

[24] Aravind, D., Senthilkumar, K., Diwahar, P., Chandrasekar, M., Kumar, T.S.M., Parameswaranpillai, J., Rajini, N., Siengchin, S. (2022). Review on coir fiber surface modification by various techniques. Coir Fiber and its Composites, 55-78. https://doi.org/10.1016/B978-0-443-15186-6.00044-8

[25] Pathariya, M.S.P., Chaudhary, V., Dwivedi, S.P., Ahlawat, C. (2025). Synthesis and dynamic performance of biorefined PLA-based bio-composites reinforced with bio-fibers. Biomass Conversion and Biorefinery, 15: 20447-20462. https://doi.org/10.1007/s13399-025-06518-4

[26] Nissar, M., Birjerane, Y.A., Patil, S., Shetty, S., Das, A. (2025). Coconut coir fiber composites for sustainable architecture: A comprehensive review of properties, processing, and applications. Journal of Composites Science, 9(10): 516. https://doi.org/10.3390/jcs9100516

[27] Mahmud, M.A., Abir, N., Anannya, F.R., Khan, A.N., Rahman, A.N.M.M., Jamine, N. (2023). Coir fiber as thermal insulator and its performance as reinforcing material in biocomposite production. Heliyon, 9(5): e15597. https://doi.org/10.1016/j.heliyon.2023.e15597

[28] Dong, Y., Ghataura, A., Takagi, H., Haroosh, H.J., Nakagaito, A.N., Lau, K.T. (2014). Polylactic acid (PLA) biocomposites reinforced with coir fibres: Evaluation of mechanical performance and multifunctional properties. Composites Part A: Applied Science and Manufacturing, 63: 76-84. https://doi.org/10.1016/j.compositesa.2014.04.003

[29] Brahmakumar, M., Pavithran, C., Pillai, R.M. (2005). Coconut fibre reinforced polyethylene composites: Effect of natural waxy surface layer of the fibre on fibre/matrix interfacial bonding and strength of composites. Composites Science and Technology, 65(3-4): 563-569. https://doi.org/10.1016/j.compscitech.2004.09.020

[30] Bakri, B., Putra, A.E.E., Mochtar, A.A., Renreng, I., Arsyad, H. (2018). Sodium bicarbonate treatment on mechanical and morphological properties of coir fibres. International Journal of Automotive and Mechanical Engineering, 15(3): 5562-5572. https://doi.org/10.15282/ijame.15.3.2018.12.0427

[31] ASTM International. (2022). ASTM D638-02: Standard test method for tensile properties of plastics. In America Society for Testing and Material. ASTM International. https://doi.org/10.1520/D0638-22

[32] Anand Kumar, S., Shivraj Narayan, Y. (2018). Tensile testing and evaluation of 3D-printed PLA specimens as per ASTM D638 type IV standard. Innovative Design, Analysis and Development Practices in Aerospace and Automotive Engineering (I-DAD 2018), 2: 79-95. https://doi.org/10.1007/978-981-13-2718-6_9

[33] dos Santos, N.V., Cavalcanti, D.K.K., Neto, J.S.S., de

Queiroz, H.F.M., Banea, M.D., Cardoso, D.C.T. (2025). Analysis of voids, interfacial and thermal properties of additively manufactured continuous natural fiber-reinforced biocomposites. Progress in Additive Manufacturing, 10(8): 5401-5422. https://doi.org/10.1007/s40964-024-00913-5

[34] Yang, D., Zhang, H., Wu, J., McCarthy, E.D. (2021). Fibre flow and void formation in 3D printing of short-fibre reinforced thermoplastic composites: An experimental benchmark exercise. Additive Manufacturing, 37: 101686. https://doi.org/10.1016/j.addma.2020.101686

[35] Vaxman, A., Narkis, M., Siegmann, A., Kenig, S. (1989). Void formation in short-fiber thermoplastic composites. Polymer Composites, 10(6): 449-453. https://doi.org/10.1002/pc.750100609

[36] Yadav, A., Rohru, P., Babbar, A., Kumar, R., Ranjan, N., Chohan, J.S., Kumar, R., Gupta, M. (2023). Fused filament fabrication: A state-of-the-art review of the technology, materials, properties and defects. International Journal on Interactive Design and Manufacturing (IJIDeM), 17(6): 2867-2889. https://doi.org/10.1007/s12008-022-01026-5

[37] Hidalgo-Salazar, M.A., Correa-Aguirre, J.P., García-Navarro, S., Roca-Blay, L. (2020). Injection molding of coir coconut fiber reinforced polyolefin blends: Mechanical, viscoelastic, thermal behavior and three-dimensional microscopy study. Polymers, 12(7): 1507. https://doi.org/10.3390/polym12071507

[38] Phengchan, P., Chaijaruwanich, A., Nakkiew, W., Pitjamit, S. (2019). Characterization and fabrication of bio-composite filaments for fused deposition modeling 3D printing. IOP Conference Series: Materials Science and Engineering, 639: 12019. https://doi.org/10.1088/1757-899X/639/1/012019

[39] Alam, M.S., Kaur, J., Khaira, H., Gupta, K. (2016). Extrusion and extruded products: Changes in quality attributes as affected by extrusion process parameters: A review. Critical Reviews in Food Science and Nutrition, 56(3): 445-473. https://doi.org/10.1080/10408398.2013.779568

[40] Mbow, M.M., Marin, P.R., Pourroy, F. (2020). Extruded diameter dependence on temperature and velocity in the fused deposition modeling process. Progress in Additive Manufacturing, 5(2): 139-152. https://doi.org/10.1007/s40964-019-00107-4

[41] Liu, W., Zhou, J., Ma, Y., Wang, J., Xu, J. (2025). Fabrication of PLA filaments and its printable performance. IOP Conference Series: Materials Science and Engineering, 275: 12033. https://doi.org/10.1088/1757-899X/275/1/012033

[42] Gichuki, J., Kareru, P.G., Gachanja, A.N., Ngamau, C. (2022). Characteristics of microcrystalline cellulose from coir fibers. Journal of Natural Fibers, 19(3): 915-930. https://doi.org/10.1080/15440478.2020.1764441

[43] Song, M.L., Yu, H.Y., Chen, L.M., Zhu, J.Y., Wang, Y.Y., Yao, J.M., Zou, Z., Tam, K.C. (2019). Multibranch strategy to decorate carboxyl groups on cellulose nanocrystals to prepare adsorbent/flocculants and pickering emulsions. ACS Sustainable Chemistry & Engineering, 7(7): 6969-6980. https://doi.org/10.1021/acssuschemeng.8b06671

[44] French, A.D. (2014). Idealized powder diffraction patterns for cellulose polymorphs. Cellulose, 21(2): 885-896. https://doi.org/10.1007/s10570-013-0030-4

[45] Sharafi, Z.S., Fathi, B., Ajji, A., Robert, M., Elkoun, S. (2022). Phase transition and crystallization behavior of grafted starch nanocrystals in PLA nanocomposites. Express Polymer Letters, 16(12): 1253-1266. https://doi.org/10.3144/expresspolymlett.2022.91

[46] Nguyen, T.L., Bedoui, F., Mazeran, P., Guigon, M. (2015). Mechanical investigation of confined amorphous phase in semicrystalline polymers: Case of PET and PLA. Polymer Engineering & Science, 55(2): 397-405. https://doi.org/10.1002/pen.23896

[47] Ghaffar, S.H., Madyan, O.A., Fan, M., Corker, J. (2018). The influence of additives on the interfacial bonding mechanisms between natural fibre and biopolymer composites. Macromolecular Research, 26(10): 851-863. https://doi.org/10.1007/s13233-018-6119-8

[48] Tao, Y., Wang, H., Li, Z., Li, P., Shi, S.Q. (2017). Development and application of wood flour-filled polylactic acid composite filament for 3D printing. Materials, 10(4): 339. https://doi.org/10.3390/ma10040339

[49] Dugvekar, M., Dixit, S. (2022). Chemical treatments for modification of the surface morphology of coir fiber: A review. Journal of Natural Fibers, 19(15): 11940-11961. https://doi.org/10.1080/15440478.2022.2048938

[50] Rosa, M.F., Chiou, B., Medeiros, E.S., Wood, D.F., Williams, T.G., Mattoso, L.H.C., Orts, W.J., Imam, S.H. (2009). Effect of fiber treatments on tensile and thermal properties of starch/ethylene vinyl alcohol copolymers/coir biocomposites. Bioresource Technology, 100(21): 5196-5202. https://doi.org/10.1016/j.biortech.2009.03.085

[51] Rosa, M.F., Chiou, B., Medeiros, E.S., Wood, D.F., Mattoso, L.H.C., Orts, W.J., Imam, S.H. (2009). Biodegradable composites based on starch/EVOH/glycerol blends and coconut fibers. Journal of Applied Polymer Science, 111(2): 612-618. https://doi.org/10.1002/app.29062

[52] Albano, C., Gonzalez, J., Ichazo, M., Kaiser, D. (1999). Thermal stability of blends of polyolefins and sisal fiber. Polymer Degradation and Stability, 66(2): 179-190. https://doi.org/10.1016/S0141-3910(99)00064-6

[53] De Rosa, I.M., Iannoni, A., Kenny, J.M., Puglia, D., Santulli, C., Sarasini, F., Terenzi, A. (2011). Poly (lactic acid)/Phormium tenax composites: Morphology and thermo-mechanical behavior. Polymer Composites, 32(9): 1362-1368. https://doi.org/10.1002/pc.21159

[54] Bajwa, D.S., Adhikari, S., Shojaeiarani, J., Bajwa, S.G., Pandey, P., Shanmugam, S.R. (2019). Characterization of bio-carbon and ligno-cellulosic fiber reinforced bio-composites with compatibilizer. Construction and Building Materials, 204: 193-202. https://doi.org/10.1016/j.conbuildmat.2019.01.068

[55] Jamadi, A.H., Razali, N., Petrů, M., Taha, M.M., Muhammad, N., Ilyas, R.A. (2021). Effect of chemically treated kenaf fibre on mechanical and thermal properties of PLA composites prepared through fused deposition modeling (FDM). Polymers, 13(19): 3299. https://doi.org/10.3390/polym13193299

[56] Manral, A., Bajpai, P.K. (2018). Analysis of Natural fiber constituents: A Review. IOP Conference Series: Materials Science and Engineering, 455: 12115. https://doi.org/10.1088/1757-899X/455/1/012115

[57] Geethamma, V.G., Joseph, R., Thomas, S. (1995). Short

coir fiber-reinforced natural rubber composites: Effects of fiber length, orientation, and alkali treatment. Journal of Applied Polymer Science, 55(4): 583-594. https://doi.org/10.1002/app.1995.070550405

[58] Gu, H. (2009). Tensile behaviours of the coir fibre and related composites after NaOH treatment. Materials & Design, 30(9): 3931-3934. https://doi.org/10.1016/j.matdes.2009.01.035

[59] Tao, Y., Liu, M., Han, W., Li, P. (2021). Waste office paper filled polylactic acid composite filaments for 3D printing. Composites Part B: Engineering, 221: 108998. https://doi.org/10.1016/j.compositesb.2021.108998

[60] Weng, Z., Wang, J., Senthil, T., Wu, L. (2016). Mechanical and thermal properties of ABS/montmorillonite nanocomposites for fused deposition modeling 3D printing. Materials & Design, 102: 276-283. https://doi.org/10.1016/j.matdes.2016.04.045

[61] Spinelli, G., Kotsilkova, R., Ivanov, E., Petrova-Doycheva, I., Menseidov, D., Georgiev, V., Di Maio, R., Silvestre, C. (2019). Effects of filament extrusion, 3D printing and hot-pressing on electrical and tensile properties of poly (lactic) acid composites filled with carbon nanotubes and graphene. Nanomaterials, 10(1): 35. https://doi.org/10.3390/nano10010035

[62] Ramezani Kakroodi, A., Cheng, S., Sain, M., Asiri, A. (2014). Mechanical, thermal, and morphological properties of nanocomposites based on polyvinyl alcohol and cellulose nanofiber from Aloe vera rind. Journal of Nanomaterials, 1(1): 903498. https://doi.org/10.1155/2014/903498

[63] Vidakis, N., Petousis, M., Michailidis, N., David, C., Mountakis, N., Papadakis, V., Sfakiotakis, E., Sagris, D., Spiridaki, M., Argyros, A. (2023). Optimized PCL/CNF bio-nanocomposites for medical bio-plotted applications: Rheological, structural, and thermomechanical aspects. Bioprinting, 36: e00311. https://doi.org/10.1016/j.bprint.2023.e00311

[64] Kumar, M.S., Farooq, M.U., Ross, N.S., Yang, C.H., Kavimani, V., Adediran, A.A. (2023). Achieving effective interlayer bonding of PLA parts during the material extrusion process with enhanced mechanical properties. Scientific Reports, 13(1): 6800. https://doi.org/10.1038/s41598-023-33510-7

[65] AhmadvashAghbash, S., Verpoest, I., Swolfs, Y., Mehdikhani, M. (2023). Methods and models for fibre–matrix interface characterisation in fibre-reinforced polymers: A review. International Materials Reviews, 68(8): 1245-1319. https://doi.org/10.1080/09506608.2023.2265701